Composition-dependent induced spin and orbital magnetic moments of Ir in Co-Ir alloys from x-ray magnetic circular dichroism

V. V. Krishnamurthy and D. J. Singh
Materials Science and Technology Division, Oak Ridge National Laboratory, Oak Ridge, Tennessee 37831, USA

N. Kawamura and M. Suzuki
SPring8/JASRI, 1-1-1 Kouto, Mikazuki, Hyogo 679-5198, Japan

T. Ishikawa
SPring8/JASRI, 1-1-1 Kouto, Mikazuki, Hyogo 679-5198, Japan
and RIKEN Harima Institute, 1-1-1 Kouto, Mikazuki, Hyogo 679-5148, Japan
(Received 27 July 2005; revised manuscript received 5 July 2006; published 15 August 2006)

X-ray magnetic circular dichroism measurements with the photon helicity modulation technique at Ir $L_{2,3}$ absorption edges and sum rule analysis show that Ir develops a composition-dependent induced spin and orbital magnetic moments in hcp $Co_{100-x}Ir_x$ (x=5,17,25,32) alloys. The total moment per Ir is found to be in the range of $0.39\mu_B$–$0.1\mu_B$—i.e., decreasing with the increase of x. The spin and orbital moments of Ir in the alloys are found to be aligned antiparallel, showing the violation of the third Hund's rule at these compositions. Electronic structure calculations of Co and Ir magnetic moments in $Co_{100-x}Ir_x$ at x=25 within the local spin density approximation illustrate that significant 3*d*-5*d* hybridization results in the formation of an induced moments at the Ir sites, with the spin moments on the order of $0.2\mu_B$–$0.3\mu_B$ that are antiparallel to the Ir orbital moment concomitant with a reduced moment on the neighboring Co sites.

DOI: 10.1103/PhysRevB.74.064411 PACS number(s): 75.25.+z, 75.30.−m, 75.50.Cc, 78.70.Dm

I. INTRODUCTION

Ferromagnetism in ordered and disordered binary transition-metal alloys is of high technological importance due to extensive applications of ferromagnets such as particulate magnetic recording and data storage media.[1] In this context, investigations of the magnetic properties of alloys of Fe and Co with 5*d* group elements such as Pt or Ir by a variety of experimental techniques is the focus of present research. In dilute alloys, 3*d* atoms such as Fe often induce a magnetic moment on the 5*d* atom through interatomic exchange interactions.[2–6] In dense alloys, apart from the interatomic exchange interactions, lattice periodicity and clustering may also play an important role in 5*d* moment formation. Investigations of the formation of induced magnetic moment on 5*d* atoms in dense alloys would be valuable to further our understanding of their magnetization properties. A direct investigation of the magnetic behavior of the 5*d* electronic states at different alloy compositions is therefore desirable.

As a result of significant experimental and theoretical developments over the past decade, x-ray magnetic circular dichroism (XMCD) spectroscopy using synchrotron radiation has emerged as a powerful technique for investigating element-specific and shell-specific magnetism in magnetic materials.[7–17] With the availability of undulator beams at high-brilliance third-generation synchrotron radiation sources, it is now possible to obtain highly monochromated and well-collimated x rays for polarization-dependent x-ray absorption spectroscopy (XAS) using a diffractive phase retarder for bistable modulation of the helicity of photons between left-circular and right-circular polarization in the hard x-ray region.[18] The advantage of XMCD measurements when using the helicity modulation technique[18] is that it has a better signal-to-noise ratio compared to conventional XMCD measurement methods. The higher sensitivity of this modulation technique enables the detection of small magnetic moments on the order of $\sim 10^{-3}\mu_B$ of 5*d* states in magnetic solids with improved accuracy.[20] This paper deals with the application of this technique to determine the composition dependence of the element-specific magnetic moment of a 5*d* ion in magnetic alloys using XMCD spectroscopy and its sum rules.[11,12]

Using XMCD, Schütz and co-workers discovered that Ir and several other 5*d* ions develop an induced magnetic moment in dilute alloys and multilayers with iron.[21–25] Ebert and Zeller calculated the electronic structure and XMCD of 5*d* impurities Os, Ir, Pt, and Au in Fe.[26] Their calculation showed that an agreement with the experimental XMCD spectra can be achieved when the spin polarization and spin-orbit coupling are treated simultaneously. XMCD at Ir $L_{2,3}$ edges has also been reported in Ir-doped CrO_2.[27] Recently, Wilhelm *et al.*, using XMCD at $L_{2,3}$ edges, discovered that the signs of the spin and orbital moment of W in multilayers with Fe violate Hund's third rule.[28] The aim of the present work is to investigate the element-specific magnetism of Ir in dense alloys with cobalt. Masumoto *et al.* have measured the magnetization in ferromagnetic $Co_{100-x}Ir_x$ alloys of hcp structure for x of 0–35.[29] They reported that the magnetic moment of the alloy decreases linearly with the increase of Ir concentration x. They explained this feature by assuming that the magnetic moments of Ir has a negative sign and that the magnetic moment of Ir and Co are composition independent. Co $L_{2,3}$- and Rh $L_{2,3}$-edge XMCD investigations of Co-Rh alloys by Harp *et al.*[30] showed that both Co and Rh have composition-dependent magnetic moments. The magnetic moment values are $\sim 1.34\mu_B$/Co and $\sim 0.64\mu_B$/Rh in

$Co_{77}Rh_{23}$ alloy and $\sim 0.45\mu_B$/Co and $\sim 0.11\mu_B$/Rh in $Co_{49}Rh_{51}$ alloy. Recent electronic structure calculations by Ostanin, Popescu, and Ebert also show that the magnetic moments of Co and Rh in CoRh alloys are composition dependent.[31] Because Rh and Ir are isoelectronic, Co and Ir are also expected to have composition-dependent magnetic moments in Co-Ir alloys. The large neutron absorption cross section of 425±2 b for Ir does not favor the application of neutron diffraction measurements for magnetic moment determination in this alloy system. To improve our understanding of the magnetism of Ir in Co-Ir alloys, it is therefore highly desirable to determine the sign of the Ir magnetic moment and its composition dependence using XMCD spectroscopy. Here, we report the magnetic behavior of Ir in disordered hcp Co-Ir alloys for the Ir composition x in the range of 5–32 investigated by Ir $L_{2,3}$ XMCD spectroscopy. We find that Ir has a composition-dependent induced spin and orbital magnetic moments in these alloys. Moreover, the net moment of Ir has a positive sign. Electronic structure calculations using the linearized augmented plane wave (LAPW) method suggest that Ir moment formation is driven by the hybridization between Ir and Co d states.

II. EXPERIMENT

Polycrystalline samples of $Co_{100-x}Ir_x$ (x=5, 17, 25, and 32) disordered alloys were prepared by arc melting. Powder samples were prepared from the ingots. Particles with diameter less than 20 μm were prepared by filtering the power samples through a 20-μm mesh. These particles were then coated on tape such that the particles are confined between layers. XMCD measurements were carried out with these tapes in the transmission mode in a field of 1.15 T at the undulator beamline BL29XU which is equipped with a liquid-N_2-cooled Si (111) double-crystal monochromator at the SPring8 synchrotron radiation facility. The Si (111) monochromater was slightly detuned to avoid the contribution from higher-order harmonics in the 11–13-keV region. Left-circularly polarized and right-circularly polarized x rays were generated by a diamond diffractive phase retarder set to make bistable oscillations around the Bragg angle θ_B. The degree of circular polarization $|P_C|$ for the experimental set up was over 90%. The XMCD spectra $\Delta\mu t$ were recorded by switching the helicity of the x rays at a rate of 40 Hz while keeping the direction of the magnetic field fixed.[18] The data were collected at room temperature.

III. RESULTS AND DISCUSSION

A. X-ray magnetic circular dichroism

We first normalized XAS such that the L_3 XAS edge jump is unity. The threshold energy E_{th} of the L_2 and L_3 XAS was determined by the maximum derivative method using the software package for extended x-ray absorption fine structure (EXAFS) data extraction and modeling, SEDEM.[19] In this method, first the energy region around the edge jump is chosen. Then the program performs a linear interpolation, computes the best possible derivative of the spectrum, and suggests the energy where a maximum appears in the derivative as the threshold energy. The derived values of threshold energies are $E_{th}(L_3)$=11 210 eV for the L_3 edge and $E_{th}(L_2)$ =12 821 eV for the L_2 edge. Then, an arc tangent function which smoothly connects the pre-edge and after-edge base lines of the XAS is calculated using the respective E_{th} value and was subtracted from the normalized XAS. The resulting difference spectra consisted of a Lorentzian-shaped peak, which is often referred to as the white line and a broad satellite. The XAS-integrated intensity μ_0 was obtained by integrating the diffence spectra of the L_3 and L_2 edges. The normalized XMCD integrals—i.e., the areas under the XMCD peaks—for L_3 and L_2 edges are obtained with the integration range of ±30 eV around the peak position E_0 of the respective edge, where $|\Delta\mu t|$ is maximum. We represent the integrated XMCD intensities as ΔL_2 and ΔL_3 for the L_2 and L_3 edges of Ir, respectively.

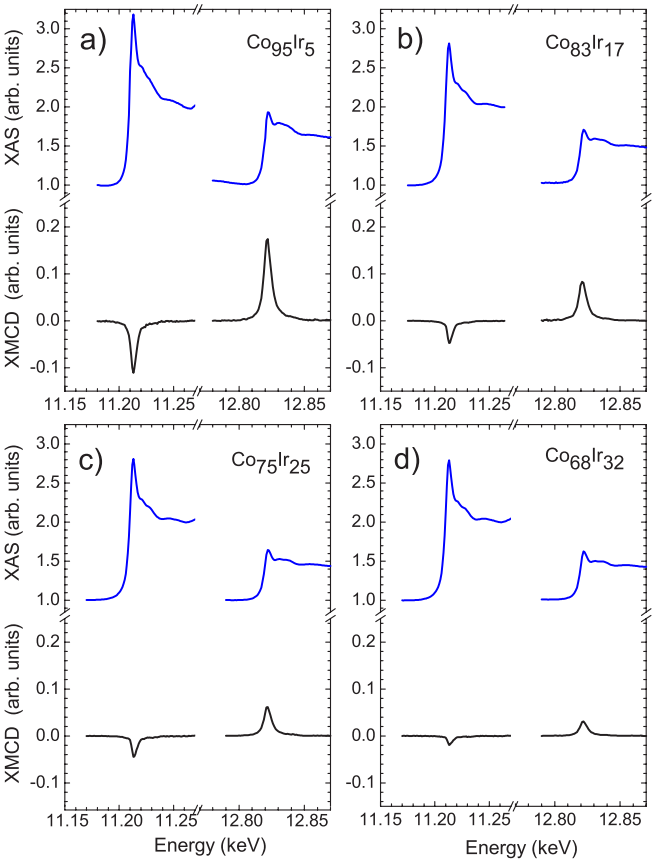

FIG. 1. (Color online) Ir L_3-edge and L_2-edge XAS and XMCD ($\Delta\mu t=\mu^+-\mu^-$) in (a) $Co_{95}Ir_5$, (b) $Co_{83}Ir_{17}$, (c) $Co_{75}Ir_{25}$, and (d) $Co_{68}Ir_{32}$ alloys.

Figure 1 shows the Ir $L_{2,3}$-edge XAS and the XMCD spectra in $Co_{100-x}Ir_x$ alloys with the Ir compositions x=5, 17, 25, and 32 (see also Fig. 2). Significant white line intensities with their peaks centered near the respective threshold energy of the edges are observed in the XAS. Magnetic circular dichroism is observed at the L_3 and L_2 edges of Ir in all the alloys, suggesting significant density of states and exchange splitting in the 5d band of Ir. These features clearly demonstrate that Ir has an ordered magnetic moment in Co-Ir alloys. The data show that the peak intensity of the XMCD

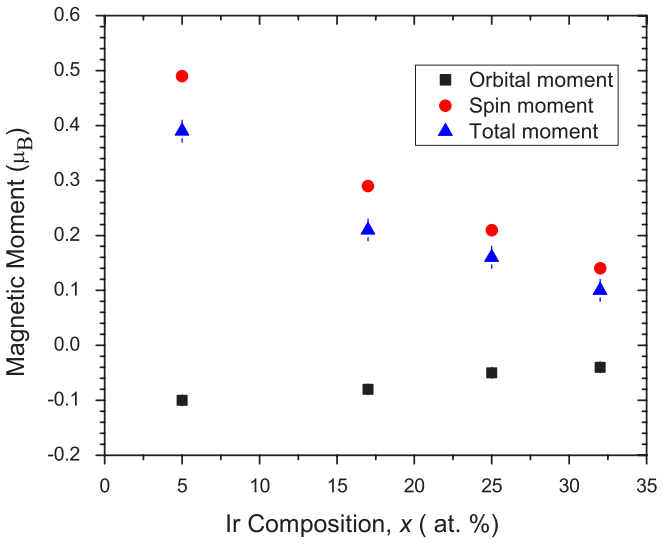

FIG. 2. (Color online) Ir composition, x dependence of the orbital magnetic moment (squares), spin magnetic moment (circles), and total magnetic moment (triangles) of Ir in $Co_{100-x}Ir_x$ alloys for $x=5-32$.

spectra $|\Delta\mu t|_{max}$ is decreasing with the increasing Ir composition x of the alloy. The orbital magnetic moment μ_{orb} and the spin magnetic moment μ_{spin} of Ir can be extracted from the XAS and XMCD spectra using the magneto-optic sum rules.[11,15] Magneto-optic sum rules relate ground-state expectation values of the spin angular momentum $\langle S_Z\rangle$ and the orbital angular momentum $\langle L_Z\rangle$ to the integrated intensities ΔL_2 and ΔL_3 of XMCD at the respective L_2 and L_3 edges and the sum of the integrated intensity of the XAS at the $L_{2,3}$ edges, μ_0. Using these notations, the orbital angular momentum sum rule and the spin angular momentum sum rule for the Ir $L_{2,3}$ edges can be written as[11,15]

$$\langle L_Z\rangle = (2/3)(\Delta L_3 + \Delta L_2)(N_h/\mu_0) \quad (1)$$

and

$$\langle S_Z\rangle + (7/2)\langle T_Z\rangle = (3/2)(\Delta L_3 - 2\Delta L_2)(N_h/\mu_0), \quad (2)$$

where N_h is the number of holes in the $5d$ orbital of Ir. $\langle T_Z\rangle$ is the magnetic-dipole operator of Ir. The threshold energy E_{th} of the L_2 and L_3 XAS was determined by the maximum derivative method. Based on the results of the electronic structure calculations for Co-Ir alloys, we assumed a $5d^7$ ground-state electronic configuration, which means $N_h=3$, for Ir in its valence d shell in Co-Ir alloys. The d^7 configuration is the atomic configuration for Ir. The values of the threshold energies E_{th} for both the edges are found to be independent of the alloy composition and support the assumed electronic configuration of Ir in all alloys.

Applying the first sum rule, defined by Eq. (1), the orbital magnetic moment of Ir, $\mu_{orb}=\langle L_Z\rangle$, could be extracted as about $-0.1\mu_B$, $-0.08\mu_B$, $-0.05\mu_B$, and $-0.04\mu_B$ at $x=5$, 17, 25, and 32, respectively. Note that the small error bars on the moment values are a result of the improvised sensitivity of the XMCD measurement using the photon helicity modulation technique. To extract μ_{spin} from the experimental XMCD spectra in noncubic compounds using the spin angular momentum sum rule, we need to use value of the magnetic-dipole operator. Our previous Ir $L_{2,3}$-edge XMCD studies of noncubic alloys and compounds showed that the expectation value of the magnetic-dipole operator, $\langle T_Z\rangle$, of Ir can be approximated by the local Lorentz field $(1/3)S_Z$.[20,32] The value of Ir moment derived from our XMCD measurement in the $Fe_{97}Ir_3$ alloy agrees with the theoretical calculation[2–4] and with the results from earlier Ir $L_{2,3}$-edge XMCD measurements in $Fe_{97}Ir_3$ alloy.[8] We therefore have used the above approximation in the second sum rule, defined by Eq. (2), to determine the spin angular momentum of Ir, $\langle S_Z\rangle$, in Co-Ir alloys. The spin magnetic moment is calculated using $\mu_{spin}=2\langle S_Z\rangle$. The results of μ_{orb}, μ_{spin}, μ_{tot}, and the ratio μ_{spin}/μ_{tot} are listed in Table I, and are shown in Fig. 2. Both the orbital moment and spin moment of Ir decrease systematically with the Ir composition. The spin moment of Ir varies from about $0.49\mu_B$ in $Co_{95}Ir_5$ alloy to about $0.14\mu_B$ in $Co_{68}Ir_{32}$ alloy. The reduction of the total moment μ_{tot} of Ir with the Ir composition x in the alloys suggests that the spin polarization of $5d$ electrons of Ir gradually shifts from Fermi energy E_F to higher energies.

TABLE I. Orbital moment μ_{orb}, spin moment μ_{spin}, and the total moment μ_{tot} of Ir in Co-Ir alloys extracted from the XMCD data. μ_{3d} is the magnetic moment per Co atom in the alloy, and μ_{tot}/μ_{3d} is the ratio of the magnetic moments of Ir with Co.

Alloy	μ_{orb} (μ_B/Ir)	μ_{spin} (μ_B/Ir)	μ_{tot} (μ_B/Ir)	μ_{3d}[a] (μ_B/3d atom)	μ_{tot}/μ_{3d}
$Co_{95}Ir_5$	−0.10(1)	0.49(2)	0.39(2)	1.63	0.24(1)
$Co_{83}Ir_{17}$	−0.08(1)	0.29(1)	0.21(2)	1.43	0.15(1)
$Co_{75}Ir_{25}$	−0.05(1)	0.21(1)	0.16(2)	1.29	0.12(1)
$Co_{68}Ir_{32}$	−0.04(1)	0.14(1)	0.10(2)	1.14	0.09(1)

[a]Values obtained by scaling the magnetic moment of the $3d$ atom (Ref. 10) with the average number of $3d$ atoms in the first-nearest-neighbor (1NN) shell in the respective alloy.

Here we investigate the correlation between the total moment μ_{tot} of Ir with the total $3d$ moment per Co atom μ_{Co} in the $Co_{100-x}Ir_x$ alloys. Taking the known value of total moment per Co, $\mu_{Co}=1.72\mu_B$ in hcp Co metal,[29] and scaling it with the number of Co in the first-nearest-neighbor (1NN) shell, we obtain the magnetic moment per Co in $Co_{100-x}Ir_x$ alloys at different x. The values of μ_{Co} obtained from such an estimate are listed along with the ratio of the magnetic moments of Ir and Co, μ_{tot}/μ_{Co}, in Table I. The total moment of Ir in $Co_{95}Ir_5$ then comes out to be $0.39\mu_B$—i.e., about 1/4 of the total $3d$ moment per Co in the alloy. This ratio is similar to the ratio reported for the $4d$ moment of Rh with the $3d$ moment of Fe in $Fe_{51}Rh_{49}$ alloy.[33] This ratio changes with alloy composition. The ratio μ_{tot}/μ_{Co} is 1/7 for $x=17$, 1/8 for $x=25$, and 1/11 for $x=32$ approximately.

The above results clearly show that the orbital moment and the spin moment of Ir in disordered Co-Ir alloys are aligned oppositely, contrary to the expectation from the third Hund's rule which states that the spin and orbital moments should be parallel for more than half-filled shells and antiparallel for less than half-filled shells for atoms.[34] This anti-

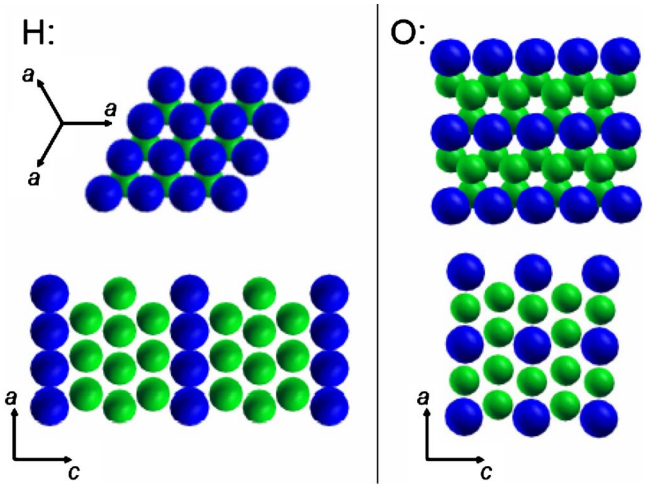

FIG. 3. (Color online) Structure of the *H* (left) and *O* (right) supercells. Co is shown as small green spheres and Ir as larger blue spheres. The layering in the *H* cell is clearly seen in the bottom panel. The top panel shows a view along the *c* axis. The three equivalent axes that are 120° apart are also displayed for the *H* supercell. The top and bottom panels for the *O* cell show a view of the Ir chains and a view perpendicular to them.

parallel alignment is also seen in our first-principles electronic structure calculations (see below). The third Hund's rule is considered to be valid in solids with some exceptions. The XMCD integral of the L_3 and L_2 edges—i.e., above the edges at ~12.86 keV—has a positive sign, suggesting that the the spin and orbital moments of Ir are antiparallel in these alloys. $L_{2,3}$-edge XMCD studies of Fe-Ir alloys, reported by Schütz *et al.*[35] and Krishnamurthy *et al.*,[32] also indicate opposite signs for the spin and orbital magnetic moments of Ir. However, it should be noted that the orbital moment of Ir in this alloy series is not a spontaneous one; rather, it is induced by the nearby 3*d* shell of Fe or Co. Our present XMCD results show that the sign of Ir orbital moment is opposite to its spin moment for a range of Ir compositions *x* from 5 to 32, indicating that the relative alignment of Ir spin and orbital moments is not affected by a change in the Co atom coordination numbers of Ir atoms. Like in the case of spin moments, it might also be possible that the induced orbital moment can be either parallel or antiparallel to the orbital moment of the magnetic 3*d* atom depending on the strength of the 3*d*-5*d* hybridization and the strength of the applied magnetic field. Recent XMCD experimental results for W in Fe/W multilayers and theoretical results for uranium in an applied magnetic field also suggest that there is a violation of Hund's third rule in metallic systems.[28,36] The magnitudes of the Ir orbital moment observed in Co-Ir alloys are much higher as compared to the orbital moment of W in Fe/W multilayers,[28] providing another example with larger values of the 5*d* orbital moment that violate the third Hund's rule. The 3*d* atom near-neighbor coordinations of 5*d* atoms are expected to be different in bulk alloys and at the 3*d*/5*d* interfaces. This is likely to affect the size of the induced magnetic moment. Some details of the role of near-neighbor atom coordinations on the size of orbital moments are pointed out below in Sec. III B. Based on the results of electronic structure calculations, Tyer *et al.* suggest that the relative alignment of spin and orbital moments in 5*d* metals is the same as in the single-impurity case, with the exception of W and Ir, which tend to violate third Hund's rule.[37] Violation of Hund's third rule has also been reported for 3*d* group magnetic ion—i.e., Cr in the $CrPt_3$ from relativistic energy-band calculations.[38] Therefore, our results in Co-Ir alloys taken together with the other results existing in the literature indicate that the hybridization between the 5*d* atom and the magnetic 3*d* atom plays an important role in the violation of Hund's third rule.

B. Electronic structure calculations

The Ir *L*-edge XMCD experimental investigations are corroborated by first-principles, local spin density approximation (LSDA) calculations. We used the general potential linearized augmented-plane-wave (APW) method,[39,40] with the APW plus local orbital modification,[41] as implemented in the WIEN2K code.[42] We did scalar relativistic calculations to obtain relaxed crystal structures and for analysis of electronic structure and hybridization, as well as self-consistent relativistic calculations at the relaxed structures, including spin-orbit, to obtain orbital moments. Two supercells with 25% Ir were treated. The structures of these two supercells are shown in Fig. 3. Both calculations used the experimental lattice parameters for this composition (a=2.573 Å, c/a =1.613), but the ordering of the Ir and Co differed. The first (denoted *H*) was a layered supercell along the hexagonal *c* axis, with pure Ir layers separated by three layers of Co. We denote the Co in the layers immediately above and below the Ir layer as Co1 and the Co in between the Co1 layers as Co2. The layering doubles the size of the unit cell along the *c* axis, and the doubled cell is also hexagonal. Therefore the notation *H* is used for this cell. The second supercell (denoted *O*) was constructed from alternating mixed (50% Co/50% Ir) and pure Co layers along the *c* axis. The Co in the mixed layer is denoted Co1, and the two inequivalent Co in the Co layer are Co2 and Co3. This type of layering doubles the size of the unit cell in the *ab* plane. The doubled cell can be views as an orthorhombic cell with its *b* axis in the *ab* plane of hexagonal base cell. For this reason, the notation *O* is used for this supercell. While there is cubic ordered Co_3Ir phase, alloys such as studied here are hexagonal. Therefore, we se-

TABLE II. Ir and Co spin moments *m*, as defined by the polarization in the LAPW spheres for the different sites in the *H* and *O* supercells, along with the coordination (n_{Co} and n_{Ir}) of the site.

Atom	Supercell	n_{Co}	n_{Ir}	m (μ_B)
Ir	*H*	6	6	0.19
Ir	*O*	10	2	0.28
Co1	*H*	9	3	1.66
Co2	*H*	12	0	1.70
Co1	*O*	8	4	1.43
Co2	*O*	10	2	1.75
Co3	*O*	8	4	1.43

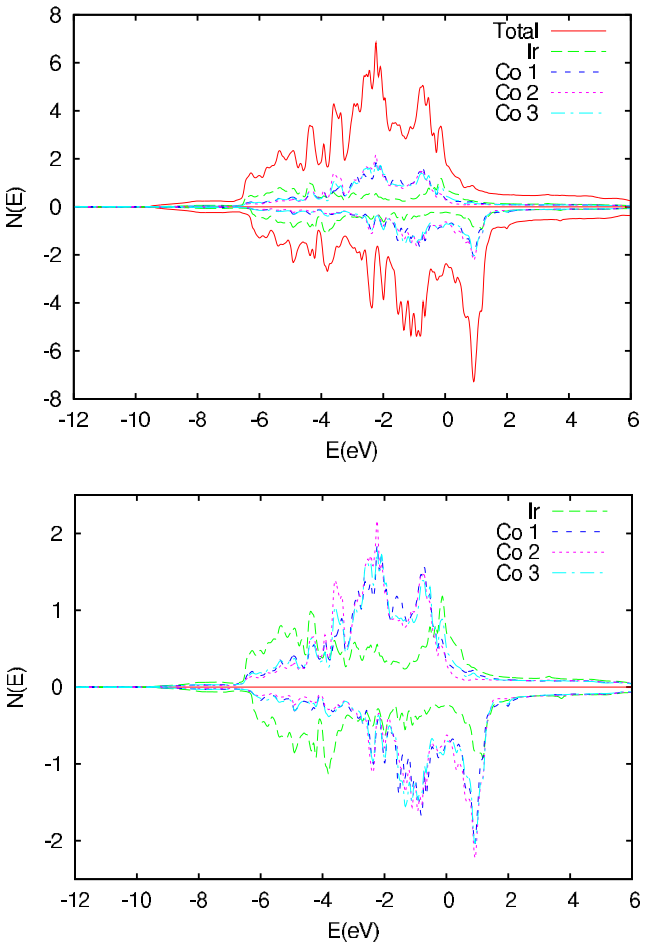

FIG. 4. (Color online) Electronic density of states (DOS) for supercell *O* (see text). The top panel shows the total DOS of the four-atom cell, while the bottom shows projections onto the various LAPW spheres (radius 2.3 bohrs) on an expanded energy scale. Majority spin is above the axis and minority below. The zero is at the Fermi energy.

lected these hexagonal base supercells, with the experimental lattice parameters to mimic the materials in the XMCD studies. In the layered supercell *H*, each Ir has six Ir nearest neighbors and six Co neighbors, while in supercell *O*, the Ir are more evenly distributed in the lattice, so that each Ir has only two Ir nearest neighbors. The atomic positions within each cell were relaxed using the calculated forces. Considering the larger size of Ir relative to Co, clustering of Ir atoms may be expected to be disfavored. Consistent with this, we find that the energy of the more uniform *O* supercell is lower than the *H* supercell by a large 0.22 eV/Ir. This is after allowing structural relaxation, which consists of a large (0.055 Å) outward displacement of the nearest-neighbor Co1 atoms in the *H* cell. Thus, because of the size difference between Ir and Co, the *O* supercell is much more representative of the alloy than the *H* supercell, and we expect that the local structure of the alloy is such that the number of Ir-Ir nearest neighbors is kept small. In any case, the qualitative magnetic behavior is the same in both supercells. The induced Ir spin moments are parallel to the Co moments, while the moments of Co atoms coordinated by Ir are reduced.

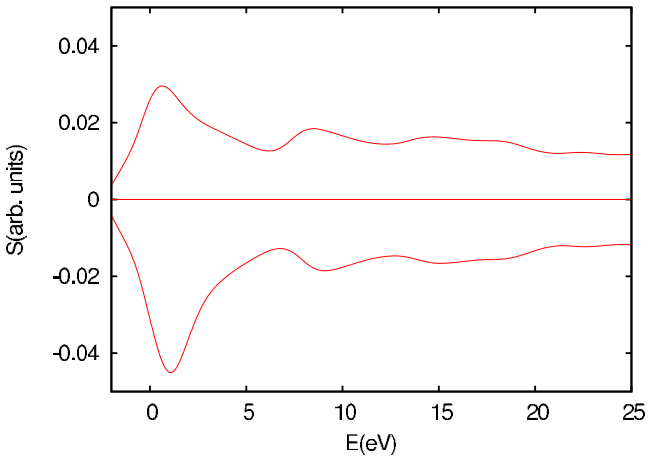

FIG. 5. (Color online) Calculated average L_3 x-ray absorption spectrum for transitions into majority (above axis) and minority (below axis) spin states, shown with a 1-eV Lorentzian broadening.

The moments associated with the various atoms in the supercells are given in Table II. The total spin magnetization of the supercells is slightly less than the sum of the atomic moments because of a small interstitial back polarization that is common in transition metals. As mentioned, the Ir moments are parallel to the Co moments. The values in the two supercells are very nearly proportional to the number of Co neighbors, consistent with a picture in which the Ir moments are induced by nearest-neighbor interactions, as expected. The Co moments also show a trend in that Co atoms with large numbers of Ir neighbors have reduced moments.

For the more realistic O supercell, the total magnetization is $4.76\mu_B$, of which $0.28\mu_B$ comes from the Ir, leaving an average $1.49\mu_B$ per Co. This large positive Ir moment is consistent with the experimental results. The calculated electronic density of states (DOS) and projections onto the LAPW spheres (radius 2.3 bohrs) are shown in Fig. 4. As may be seen, relative to the Co, the Ir contribution to the DOS within 2 eV of the Fermi energy E_F is generally similar in shape, but smaller in magnitude, reflecting the broader *d* bands of Ir. The exchange splitting of the Ir *d* states near E_F is substantial. This reflects Co-Ir hybridization. The mechanism for the Ir moment formation is therefore hybridization between Ir and Co *d* states. Aligned Ir and Co moments with substantial Ir exchange splitting favors electron hopping between Co and Ir, which reduces the kinetic energy of the system. Because of the broader Ir bands, which leads to both a majority-spin Ir *d* character at E_F and a reduced minority-spin DOS relative to Co, the induced Ir moments are much smaller than the Co moments. Nonetheless, due to of the similar shape of the Ir and Co DOS and the parallel alignment of their moments, the Ir x-ray absorption is mostly from the minority-spin channel. The calculated average spin-decomposed Ir L_3 absorption spectrum, shown in Fig. 5, has a similar overall structure to the experimental spectra and is in fact dominated by transitions to the minority-spin *d* states up to 2 eV above the edge. The smaller near-edge peak in the majority channel reflects the fact that unlike Co, there is significant majority Ir *d* character at E_F.

We also did calculations for both supercells, including spin-orbit with the magnetization direction along various di-

rections, specifically in the *ab* plane and along the *c* axis for the *H* cell, which is the cell doubled along *c*, and for the Ir chain direction, perpendicular to the Ir chain direction in the *ab* plane, and along the *c* axis for the *O* cell, which is the cell doubled in the *ab* plane. In all cases, we find Ir orbital moments opposite to the spin moment, in accordance with the experimental results. The average orbital moment on Co is $+0.078\mu_B$. Although the calculated Ir and Co orbital moments may be underestimated due to the limitations of the LSDA, the sign and relative magnitudes should be reliable.[43] With *M* along the *c*-direction easy axis of bulk Co, the values of the Ir orbital moment were $-0.027\mu_B$ and $-0.29\mu_B$ for the *H* and *O* supercells, respectively. The Ir orbital moment values for the other orientations of the magnetization were $-0.024\mu_B$ (*H* supercell, *M* in the *ab* plane), $-0.32\mu_B$ (*O* cell, *M* in the basal plane, perpendicular to Ir chains), and notably enhanced, $-0.062\mu_B$ (*O* supercell, *M* along Ir chains). The orbital moment magnetism of Ir can be understood by considering that the Ir atoms are arranged in chains and are surrounded by Co atoms. The size of the orbital moment on Ir depends on the Co coordination of Ir atoms and the orientation of the magnetization vector with respect to the direction of the Ir crystal field. For these reasons, there is a strong difference between the Ir orbital moment values in the two cells. The larger enhancement found in the *O* cell reflects the orbital ordering associated with compression of the Ir-Ir bonds along this direction. While this is an artifact of this supercell in relation to disordered alloys, it may be relevant for constructing nanostructures with large orbital moments and anisotropy. In any case, these results support the experimental finding of antiparallel induced spin and orbital moments on the Ir sites.

IV. CONCLUSIONS

In conclusion, XMCD measurements using the helicity modulation technique at Ir $L_{2,3}$ absorption edges demonstrate that Ir has composition-dependent induced spin and orbital magnetic moments in disordered hcp Co-Ir alloys. The total moment of Ir displays a scaling with the size of the 3*d* moment in the alloy. First-principles local spin density calculations show that the spin moment and the orbital moment of Ir are aligned antiparallel, in agreement with our Ir $L_{2,3}$-edge XMCD experimental results. The hybridization between Co 3*d* and Ir 5*d* states plays a role in 5*d* moment formation in the alloys. These results will have significant implications in understanding the magnetic properties, such as magnetic anisotropy, of Ir and possibly some other 5*d* group atoms in alloys.

ACKNOWLEDGMENTS

Oak Ridge National Laboratory is managed by UT-Battelle, LLC, for the U.S. Department of Energy under the Contract No. DE-AC05-00OR22725. The authors would like to acknowledge J. L. Robertson and J. Velev for very helpful discussions.

[1] S. Sun, C. B. Murray, D. Weller, L. Folks, and A. Moser, Science **287**, 1989 (2000).
[2] I. A. Campbell, Proc. Phys. Soc. London **89**, 71 (1966).
[3] I. A. Campbell, J. Phys. C **1**, 687 (1968).
[4] H. Akai, Hyperfine Interact. **43**, 255 (1988).
[5] G. Schütz, R. Wienke, W. Wilhelm, W. Wagner, P. Kienle, R. Zeller, and R. Frahm, Z. Phys. B: Condens. Matter **75**, 495 (1989).
[6] R. Wienke, G. Schütz, and H. Ebert, J. Appl. Phys. **69**, 6147 (1991).
[7] G. Schütz, W. Wagner, W. Wilhelm, P. Kienle, R. Zeller, R. Frahm, and G. Materlik, Phys. Rev. Lett. **58**, 737 (1987).
[8] G. Schütz, M. Knülle, R. Weinke, and W. Wilhelm, Z. Phys. B: Condens. Matter **73**, 495 (1988).
[9] G. van der Laan, B. T. Thole, G. A. Sawatzky, J. B. Goedkoop, J. C. Fuggle, J. M. Estéva, R. Karnatak, J. P. Remeika, and H. A. Dabkowska, Phys. Rev. B **34**, 6529 (1986).
[10] C. T. Chen, F. Sette, Y. Ma, and S. Modesti, Phys. Rev. B **42**, R7262 (1990).
[11] B. T. Thole, P. Carra, F. Sette, and G. van der Laan, Phys. Rev. Lett. **68**, 1943 (1992); P. Carra, B. T. Thole, M. Altarelli, and Xindong Wang, Phys. Rev. Lett. **70**, 694 (1993).
[12] G. Y. Guo, Phys. Rev. B **57**, 10295 (1998).
[13] Y. Wu, J. Stöhr, B. D. Hermsmeier, M. G. Samant, and D. Weller, Phys. Rev. Lett. **69**, 2307 (1992).
[14] J. G. Tobin, G. D. Waddill, and D. P. Pappas, Phys. Rev. Lett. **68**, 3642 (1992); J. G. Tobin, G. D. Waddill, A. F. Jankowski, P. A. Sterne, and D. P. Pappas, Phys. Rev. B **52**, 6530 (1995).
[15] C. T. Chen, Y. U. Idzerda, H.-J. Lin, N. V. Smith, G. Meigs, E. Chaban, G. H. Ho, E. Pellegrin, and F. Sette, Phys. Rev. Lett. **75**, 152 (1995).
[16] J. Vogel, A. Fontaine, V. Cros, F. Petroff, J.-P. Kappler, G. Krill, A. Rogalev, and J. Goulon, Phys. Rev. B **55**, 3663 (1997).
[17] W. Grange, I. Galanakis, M. Alouani, M. Maret, J.-P. Kappler, and A. Rogalev, Phys. Rev. B **62**, 1157 (2000).
[18] M. Suzuki, N. Kawamura, M. Mizumaki, A. Urata, H. Maruyama, S. Goto, and T. Ishikawa, Jpn. J. Appl. Phys., Part 2 **37**, L1488 (1998); J. Synchrotron Radiat. **6**, 190 (1999).
[19] D. Aberdam, software package for EXAFS data extraction and modeling (SEDEM), http://www.esrf.fr/computing/scientific/exafs/sedem.html
[20] V. V. Krishnamurthy, N. Kawamura, M. Suzuki, T. Ishikawa, G. J. Mankey, P. Raj, A. Satyamoorthy, Amish G. Joshi, and S. K. Malik, Phys. Rev. B **68**, 214413 (2003).
[21] G. Schütz, S. Stähler, M. Knülle, P. Fischer, S. Parkin, and H. Ebert, J. Appl. Phys. **73**, 6430 (1993).
[22] S. Stähler, G. Schütz, P. Fischer, M. Knülle, S. Rüegg, S. Parkin, H. Ebert, and W. B. Zeper, J. Magn. Magn. Mater. **121**, 234 (1993).
[23] W. J. Antel, Jr., M. M. Schwickert, Tao Lin, W. L. O'Brien, and G. R. Harp, Phys. Rev. B **60**, 12933 (1999).
[24] F. Wilhelm, P. Poulopoulos, G. Ceballos, H. Wende, K. Baber-

schke, P. Srivastava, D. Benea, H. Ebert, M. Angelakeris, N. K. Flevaris, D. Niarchos, A. Rogalev, and N. B. Brookes, Phys. Rev. Lett. **85**, 413 (2000).
[25] P. Poulopoulos, F. Wilhelm, H. Wende, G. Ceballos, K. Baberschke, D. Benea, H. Ebert, M. Angelakeris, N. K. Flevaris, A. Rogalev, and N. B. Brooks, J. Appl. Phys. **89**, 3874 (2001).
[26] H. Ebert and R. Zeller, Phys. Rev. B **42**, 2744 (1990).
[27] P. Dalmas de Réotier, J. P. Sanchez, M. Belakhovsky, J. B. Goodkoop, J. Goulon, C. Goulon-Ginet, and G. Demezeau, J. Phys. IV **7**, C2-451 (1997).
[28] F. Wilhelm, P. Poulopoulos, H. Wende, A. Scherz, K. Baberschke, M. Angelakeris, N. K. Flevaris, and A. Rogalev, Phys. Rev. Lett. **87**, 207202 (2001).
[29] H. Masumoto, K. Watanabe, and K. Inagawa, Trans. Jpn. Inst. Met. **17**, 592 (1976).
[30] G. R. Harp, S. S. P. Parkin, W. L. O'Brien, and B. P. Tonner, Phys. Rev. B **51**, R12037 (1995).
[31] S. Ostanin, V. Poposcu, and H. Ebert, J. Phys.: Condens. Matter **13**, 3895 (2001).
[32] V. V. Krishnamurthy, M. Suzuki, N. Kawamura, T. Ishikawa, and Y. Kohori, Physica B **312–313**, 647 (2002).
[33] J. Chaboy, Fernando Bartolomé, M. R. Ibarra, C. I. Marquina, P. A. Algarabel, Andrei Rogalev, and Claus Neumman, Phys. Rev. B **59**, 3306 (1999).
[34] N. W. Ashcroft and N. D. Mermin, *Solid State Physics* (Halt, Rinehart and Winston, Philadelphia, 1976).
[35] G. Schütz, M. Knulle, and H. Ebert, Phys. Scr. **T49A**, 302 (1993).
[36] A. Hjelm, O. Eriksson, and B. Johansson, Phys. Rev. B **71**, 1459 (1993).
[37] R. Tyer, G. van der Laan, W. M. Temmerman, Z. Szotek, and H. Ebert, Phys. Rev. B **67**, 104409 (2003).
[38] P. M. Oppeneer, I. Galanakis, A. Grechnev, and O. Eriksson, J. Magn. Magn. Mater. **240**, 371 (2002).
[39] D. J. Singh, *Planewaves, Pseudopotentials and the LAPW Method* (Kluwer Academic, Boston, 1994).
[40] D. Singh, Phys. Rev. B **43**, 6388 (1991).
[41] E. Sjostedt, L. Nordstrom, and D. J. Singh, Solid State Commun. **114**, 15 (2000).
[42] P. Blaha, K. Schwarz, G. K. H. Madsen, D. Kvasnicka, and J. Luitz, computer code WIEN, Technical University of Vienna, Vienna, 2002.
[43] G. H. O. Daalderop, P. J. Kelly, and M. F. H. Schuurmans, Phys. Rev. B **41**, 11919 (1990).